International Journal of Nanomedicine

Dovepress
open access to scientific and medical research

Open Access Full Text Article

ORIGINAL RESEARCH

Cell type-dependent uptake, localization, and cytotoxicity of 1.9 nm gold nanoparticles

This article was published in the following Dove Press journal:
International Journal of Nanomedicine
31 May 2012
Number of times this article has been viewed

Jonathan A Coulter[1]
Suneil Jain[2]
Karl T Butterworth[2]
Laura E Taggart[2]
Glenn R Dickson[2]
Stephen J McMahon[3]
Wendy B Hyland[1]
Mark F Muir[3]
Coleman Trainor[2]
Alan R Hounsell[2,4]
Joe M O'Sullivan[2,4]
Giuseppe Schettino[2]
Fred J Currell[3]
David G Hirst[1]
Kevin M Prise[2]

[1]School of Pharmacy, McClay Research Centre, [2]Centre for Cancer Research and Cell Biology, [3]School of Mathematics and Physics, Queens University Belfast, [4]Belfast Health and Social Care Trust, Belfast, Ireland

Background: This follow-up study aims to determine the physical parameters which govern the differential radiosensitization capacity of two tumor cell lines and one immortalized normal cell line to 1.9 nm gold nanoparticles. In addition to comparing the uptake potential, localization, and cytotoxicity of 1.9 nm gold nanoparticles, the current study also draws on comparisons between nanoparticle size and total nanoparticle uptake based on previously published data.

Methods: We quantified gold nanoparticle uptake using atomic emission spectroscopy and imaged intracellular localization by transmission electron microscopy. Cell growth delay and clonogenic assays were used to determine cytotoxicity and radiosensitization potential, respectively. Mechanistic data were obtained by Western blot, flow cytometry, and assays for reactive oxygen species.

Results: Gold nanoparticle uptake was preferentially observed in tumor cells, resulting in an increased expression of cleaved caspase proteins and an accumulation of cells in sub G_1 phase. Despite this, gold nanoparticle cytotoxicity remained low, with immortalized normal cells exhibiting an LD_{50} concentration approximately 14 times higher than tumor cells. The surviving fraction for gold nanoparticle-treated cells at 3 Gy compared with that of untreated control cells indicated a strong dependence on cell type in respect to radiosensitization potential.

Conclusion: Gold nanoparticles were most avidly endocytosed and localized within cytoplasmic vesicles during the first 6 hours of exposure. The lack of significant cytotoxicity in the absence of radiation, and the generation of gold nanoparticle-induced reactive oxygen species provide a potential mechanism for previously reported radiosensitization at megavoltage energies.

Keywords: endocytosis, proliferation, reactive oxygen species, transmission electron microscopy

Introduction

The field of nanomedicine covers a disparate array of research, with applications ranging from the use of quantum dots for enhanced in vivo imaging to the use of gold nanowires for highly targeted payload delivery at the subcellular level.[1,2]

Few nanostructures have received as much attention as gold nanoparticles, due to the chemically inert nature of gold and the relative ease with which the surface chemistry can be manipulated for downstream applications.[3–6] Furthermore, gold nanoparticles have been investigated in various contexts in relation to cancer diagnosis and treatment, including as a delivery vehicle for several chemotherapeutic agents, as a contrast agent for enhanced imaging, and for thermal ablation therapy.[7–11]

Utilizing the differential absorption coefficient of a high atomic number (Z) material, such as gold, compared with soft tissue has shown potential as a radiosensitizing strategy through increased local dose deposition as a result of the generation of

Correspondence: Jonathan Coulter
School of Pharmacy, Queen's University Belfast, 97 Lisburn Rd, Belfast, BT9 7BL, Ireland
Tel +44 028 9097 2307
Fax +44 028 9097 2776
Email j.coulter@qub.ac.uk

secondary electron species.[12–14] A tissue modeling study using gold foil reported a dose enhancement factor of 50 due to the production of secondary electrons generated from low-energy photon irradiation.[15] Subsequent progression to produce smaller particles, thereby increasing the gold surface area to volume ratio, resulted in the production of gold particles in the nanometer range. Hainfeld et al[6] detailed the first study using 1.9 nm gold nanoparticles as radiosensitizers. The gold nanoparticles were administered by tail vein injection and resulted in a 66% increase in the one-year survival of mice bearing EMT-6 mammary tumors when pretreated with a single intravenous dose of gold nanoparticles and irradiated with 250 kVp x-rays, compared with radiotherapy alone. Furthermore, the effects occurred in a dose-dependent manner, with no animals exhibiting significant gold nanoparticle-induced cytotoxicity.[6] More recently, interest has shifted towards the dependence of radiosensitization on the energy of the radiation source, with particular emphasis on clinically relevant energies. Corroborating both the modeled predictions and the findings of Chithrani et al,[16] we observed a greater radiosensitization potential for cells irradiated with lower energy beams, achieving sensitizer enhancement ratios of 1.41 and 1.29 for 160 kVp and 6 MV photon sources, respectively.[16,17] However, discrepancies between the size of the modeled enhancement (10–2000-fold, dependent on beam energy) and the observed findings suggest a more complex role for various biological interactions, which remains poorly understood.[18] To provide an insight into the biological processes governing radiosensitization, numerous variables, including nanoparticle size, shape, and charge, have been investigated to determine their impact on nanoparticle uptake, intracellular distribution, and radiosensitization potential. Chithrani et al[19] demonstrated the contribution of nanoparticle size to gold nanoparticle uptake by reporting a three-fold preferential uptake of 50 nm gold nanoparticles compared with 100 nm gold nanoparticles over the same time period. A shift in the absorption spectra following incubation of the gold nanoparticles in culture medium containing 10% serum indicated binding of serum protein to the surface of the nanoparticles. The nonspecific binding of serum proteins resulted in surface modification, increasing intracellular uptake by receptor-mediated endocytosis.[19,20]

Uncertainty remains as to whether gold nanoparticles induce a cytotoxic response, with some authors attributing cytotoxicity to individual preparations or nanoparticle size, while others conclude that gold nanoparticles do not induce any immunogenic or cytotoxic effects.[21–24] A recent study investigating 16 nm gold nanoparticle stability and cytotoxicity in K562 human erythroleukemia cells following gamma irradiation reported minimal cytotoxicity (<10%) at low gold nanoparticle concentrations (<100 μg/mL), increasing significantly to 58% at the highest gold nanoparticle concentration, demonstrating the dose-dependent nature of gold nanoparticle cytotoxicity.[25]

In this study, we aimed to investigate in detail the physical parameters contributing to radiosensitization. These include precise measurement of the uptake potential affecting different cell types and the intracellular distribution of gold nanoparticles, because localization near to critical sites such as DNA would significantly modify the sensitivity to radiation treatment. Furthermore, we investigated the impact of 1.9 nm gold nanoparticles on functional outputs, including cytotoxicity measured by changes in proliferative index, 3-(4,5-dimethylthiazol-2-yl)-2,5-diphenyltetrazolium bromide (MTT, Sigma, St Louis, MO) and clonogenic assays. The colony-forming assay was also used to determine the extent to which 1.9 nm gold nanoparticle treatments could sensitize cell line models to a single 3 Gy x-ray dose. Finally, we investigated if 1.9 nm gold nanoparticles could induce production of reactive oxygen species, thereby potentially providing a biological mechanism for gold nanoparticle-induced cell death and reported radiosensitization at MV photon energies.[17]

Materials and methods

Cell culture

Human DU145 prostate cancer cells, MDA-MB-231 breast cancer cells, and L132 lung epithelial cells were cultured in Roswell Park Memorial Institute (RPMI) 1640, Dulbecco's modified Eagle's medium, and Minimum Essential Medium, respectively. All cells were purchased from the American Type Culture Collection. All media were supplemented with 10% fetal bovine serum and 1% penicillin-streptomycin (Invitrogen, Carlsbad, CA). All cells were maintained in monolayers in a tissue culture incubator at 37°C with 5% CO_2/95% air and subcultured every 3–4 days to maintain exponential growth.

1.9 nm gold nanoparticles

1.9 nm spherical gold nanoparticles (Aurovist™) used in previous radiation studies, were purchased from Nanoprobes Inc (Yaphank, NY).[6,7,26,27] Gold nanoparticles were suspended in molecular grade sterile water (Sigma), filtered through a 0.2 μm filter, and stored at –20°C as per the manufacturer's instructions at a concentration of 2.4 mM (10% by mass). This stock suspension was diluted appropriately to the required concentration in culture medium immediately prior

to use. Gold concentrations were confirmed using inductively coupled plasma atomic emission spectroscopy (ICP-AES).

Gold nanoparticle characterization

A 2 µL aliquot of the gold nanoparticle suspension was pipetted onto a mesh formvar-carbon coated copper transmission electron microscopy (TEM) grid (Polysciences Inc, Warrington, PA) and allowed to air-dry. Samples were imaged using a field emission TEM (Technai F20), an established method for gold nanoparticle size quantification.[21] Gold nanoparticle size was determined using open-source image analysis software (Image J). A minimum of 400 nanoparticles were analyzed.

Inductively coupled plasma-atomic emission spectroscopy

First, 7.5×10^4 cells were plated for 24 hours, then exposed to 1.9 nm gold nanoparticles for 1–24 hours, washed three times in phosphate-buffered saline, trypsinized, counted, and digested in 0.5 mL of aqua regia (one part 100% nitric acid to three parts 100% hydrochloric acid). Each sample volume was made up to 5 mL with distilled water, and the gold content was determined using a Perkin Elmer Optima 4300 DV ICP-AES, which measures absolute quantification of elemental gold with parts per billion sensitivity.

Calculating the number of gold nanoparticles/cell

The amount of gold per cell was calculated from the total gold content per sample determined by ICP-AES, and the number of cells in each sample counted with a Z1 Coulter particle counter (Beckman Coulter Inc, Fullerton, CA). A gold atom has a radius of 0.14 nm. The length (L) and volume (F) of a gold unit cell can thus be calculated as:

$$2L^2 = (4r)^2$$

$$L = \sqrt{8r^2} = 407 \text{ pm } (r = 0.14 \text{ nm})$$

$$\text{Volume of gold cell} = L^3 = 6.74 \times 10^7 \text{ pm}^3 \text{ or } 67.3 \text{ Å}^3$$

Gu et al[28] calculated the number of gold atoms per nanoparticle using the following formula:

$$n = \frac{\frac{4}{3}\pi\left(\frac{D}{2}\right)^3}{F} \times 4$$

where n = number of gold nanoparticles, D = gold nanoparticle diameter, and F = volume of a gold cell.[28]

Therefore, a 1.9 nm gold nanoparticle is calculated to contain about 200 gold atoms.

The volume of a typical cell was calculated assuming a spherical cell to allow an approximate estimation of intracellular gold nanoparticle concentration. The typical diameter of an MDA-MB-231 cell was estimated (n = 20) using TEM at 13.5 µm. The volume is therefore:

$$V = \frac{4}{3}\pi r^3$$

where V is the volume of the cell and r is the radius (6.75 µm). The volume is therefore 1288.3 μm^3.

The concentration C is calculated by:

$$C = \frac{m}{V}$$

where m = mass of gold/cell.

Confocal microscopy of immunogold

Alexa Fluor® 488 Fluoronanogold™ was purchased from Nanoprobes Inc. This product consists of 1.4 nm gold nanoparticles conjugated via a hinge thiol to Alexa Fluor 488 (Molecular Probes, Eugene, OR) enabling visualization of gold nanoparticle conjugates using confocal microscopy. Then 1×10^4 cells were plated in 4-well Labtek chamber slides (Nunc, Waltham, MA) and allowed to adhere for 24 hours. The medium was removed, cells washed with phosphate-buffered saline, and fresh medium was added containing Fluoronanogold 8 µg/mL for 1–24 hours. The cell medium and gold nanoparticles were removed and the cells were washed three times in chilled phosphate-buffered saline. Ice-cold 50% methanol to 50% acetone was added for 8 minutes at 4°C to fix the cells, which were then mounted with Vectashield and 4,6-diamidino-2-phenylindole (DAPI, Vector Laboratories, Burlingame, CA). Images were acquired using a Leica SP5 confocal microscope with a FITC filter exciting at 488 nm and emitting at 514 nm and a ultraviolet filter exciting at 370 nm and emitting at 440 nm wavelengths for DAPI.

TEM and energy dispersive x-ray spectroscopy

First, 1.5×10^5 cells were plated for 24 hours, and then exposed to 1.9 nm gold nanoparticles for a further 24 hours. Cells were washed twice in phosphate-buffered saline, trypsinized, pelleted, and fixed in 4% glutaraldehyde in 0.1 M sodium cacodylate for 4 hours. Cells were post-fixed in 1% osmium tetroxide in sodium cacodylate for one hour and

washed in 0.1 M sodium cacodylate for 2 hours. Cell pellets were then dehydrated in a graded series of ethanol (30%, 60%, 70%, 90%, and 100%), exposed to propylene oxide for 10 minutes, infiltrated with 1:1 ratio of propylene oxide and resin for one hour, and embedded in agar resin overnight. The resin was allowed to polymerize at 60°C for 48 hours, cooled for 12 hours, and sectioned at 60–70 nm thickness using a Reichert Ultracut E ultramicrotome. Sections were placed on mesh copper support grids, stained with uranyl acetate for 12 minutes, lead citrate for 10 minutes, and imaged with a Phillips CM 100 TEM (Eindhoven, The Netherlands) at 100 kV for lower resolution imaging and an FEI Technai F20 TEM for higher resolution imaging. To confirm the presence of gold, the FEI Technai F20 TEM was used in scanning TEM mode for energy dispersive x-ray spectroscopy.

Cell growth assay

Initially, 1×10^4 cells were plated for 24 hours, and then treated with 0 μM, 2.4 μM, or 12 μM (0 μg/mL, 100 μg/mL, or 500 μg/mL, respectively) 1.9 nm gold nanoparticles for 24 hours, washed twice in phosphate-buffered saline, and incubated in fresh culture medium. Cell numbers in the control and gold nanoparticle exposed samples were counted at hours 0, 24, 48, and 72 using a Z1 counter (Beckman Coulter Inc). Results were fitted to an exponential fit using Prism 5.0 (GraphPad Software, San Diego, CA).

MTT cell viability assay

First, 5.0×10^3 MDA-MB-231, DU145, or L132 cells were plated in each well of a 96-well plate and incubated for 24 hours to adhere. The culture medium was replaced with fresh medium containing various concentrations of gold nanoparticles ranging from 10 μg/mL to a maximum of 2 mg/mL and incubated for a further 24 hours. Cells were then exposed to 30 μL of MTT and incubated for a further 4 hours, after which the medium with MTT was removed, the cells were washed once with phosphate-buffered saline, and then lysed with 170 μL dimethyl sulfoxide. Plates were read using a GENios colorimetric plate reader at 540 nm with results plotted relative to unexposed control cells using Prism 5.0 (GraphPad Software, San Diego, CA). Statistical analysis was performed using the Student's *t*-test (n = 4).

Gold nanoparticles and radiation

A total of 7.5×10^4 cells were plated in 35 mm^2 dishes containing culture medium supplemented with fetal bovine serum and 1% penicillin-streptomycin for 24 hours. The medium was removed, and cells were exposed to fresh medium containing 1.9 nm gold nanoparticles for 24 hours, then irradiated with 3 Gy x-rays. After irradiation, cells were washed twice in phosphate-buffered saline, trypsinized, diluted four-fold to allow sufficient plating volume, vortexed at 1800 rpm for 10 seconds to achieve a single cell suspension, counted, and replated for survival analysis using the clonogenic assay technique described by Puck and Marcus.[29] Colonies were stained with 0.4% crystal violet and counted using a Colcount colony counter (Oxford Optronix, Abingdon, UK). Plating efficiency was calculated as the ratio of colonies to cells seeded. The surviving fractions were calculated as the plating efficiency of the treated group divided by the plating efficiency of the untreated control cells. The statistical analysis was performed using the Student's *t*-test (n = 4).

Western blotting

First, 7.5×10^4 cells were plated in 35 mm^2 dishes in culture medium supplemented with fetal bovine serum and 1% penicillin-streptomycin for 24 hours. Fresh medium containing 12 μM gold nanoparticles was added for various time points up to 48 hours. Whole cell extracts were collected by scraping in 250 μL of Laemmli buffer (Sigma) and stored at −20°C. Before use, cell lysates were heated to 90°C for 10 minutes to denature proteins. The Novex Mini-cell system (Invitrogen) was used for protein separation and transfer. A 10% NuPAGE Bis-Tris gel (Invitrogen) was submerged in 1 × 3-(N-morpholino)propanesulfonic acid (MOPS) running buffer (Invitrogen). A 20 μL sample was loaded with 10 μL SeeBlue Plus2 prestained protein standard (Invitrogen), and electrophoresed at 200 V for 2 hours. Proteins were transferred to Hybond-C nitrocellulose membrane (GE Healthcare Bio-Sciences UK Ltd, Little Chalfont, UK), immersed in 1 × transfer buffer (Invitrogen) and transferred at 25 V for 1.5 hours. Membranes were blocked in 1% blocking solution for 20 minutes and incubated overnight in 1:1000 primary antibody and 1% blocking solution at 4°C. Human-specific primary antibodies used were poly(ADP-ribose)polymerase (PARP), cleaved PARP, caspase-9, cleaved caspase-9 and β-actin (Cell Signaling 9542, 9541, 9502, 9501, and Sigma A3583, respectively).

Membranes were washed three times for 5 minutes in phosphate-buffered saline and 0.1% Tween-20, followed by a final 5-minute wash in phosphate-buffered saline, and then incubated in 1:5000 antirabbit secondary antibody (GE Healthcare Bio-Sciences UK Ltd) in 1% blocking solution at room temperature for 2 hours. Membranes were washed three times in phosphate-buffered saline, treated

with Supersignal Western blotting detection reagent (MSC, Pierce, Rockford, IL) and exposed to x-ray film in the dark room. Digital images were acquired using a Canon Powershot 7.1 MP camera.

Flow cytometry

First, 7.5×10^4 cells were plated in 35 mm^2 dishes for 24 hours, exposed to 12 µM gold nanoparticles in culture medium for 24 hours, trypsinized, centrifuged, and fixed in 70% ethanol at 4°C for one hour. Cells were resuspended in phosphate-buffered saline containing 50 µg/mL of propidium iodide and 10 µg/mL RNase, and incubated at 37°C for 30 minutes. Samples were analyzed using a FACSCalibur flow cytometer and CELL-Quest software (Becton-Dickinson, BD Biosciences, Franklin Lakes, NJ). In total, 10,000 cells were analyzed per sample.

Measurement of reactive oxygen species

Cells were seeded into 6-well plates and allowed to adhere overnight before incubating with 12 µM gold nanoparticles. In addition, H_2O_2 was used at a concentration of 2.5 mM to act as a positive control for the formation of reactive oxygen species. At either 1 hour or 24 hours following treatment, nanoparticle-containing medium was removed and replaced with serum-free medium containing 5 µM 5-6-chloromethyl-2′7′-dichlorodihydrofluorescein diacetate acetyl ester (2DCFDA, Molecular Probes, Invitrogen). Cells were incubated at 37ºC for 30 minutes, washed with phosphate-buffered saline, and detached using cell dissociation buffer (Sigma, Gillingham, UK). Samples were analyzed using a FACSCalibur flow cytometer and CELL-Quest software (Becton, Dickinson and Company, Oxford, UK). 10,000 cells were analyzed per sample; values are expressed as the mean ± standard error. Statistical significance was determined using a *t*-test.

Results

1.9 nm gold nanoparticle characterization

Commercially produced 1.9 nm gold nanoparticles were imaged by TEM to determine the size distribution for comparison with the manufacturer's specification (Figure 1). Four hundred particles were measured using Image J analysis software. On analysis, 70.3% of the particles ranged between 1.5 nm and 2.5 nm, with a mean particle diameter of 2.2 ± 0.2 nm (Figure 1).

ICP-AES determination of gold nanoparticle uptake

Figure 2 shows the cellular uptake of gold nanoparticles as determined by ICP-AES. Gold nanoparticle uptake occurred in a dose-dependent and time-dependent manner with a steady increase in the number of nanoparticles per cell up to the 6-hour time point, and reaching a plateau at 6 hours. Increasing the concentration of gold nanoparticles in the culture medium from 2.4 µM to 12 µM significantly increased the number of intracellular nanoparticles by 73% and 58% for L132 and DU145 cells, respectively, following a 24-hour exposure. The slope of the curve during the first 6 hours of exposure was used to determine the rate of uptake. Exposure of DU145 and L132 cells to 12 µM gold nanoparticles resulted in comparable mean uptake rates of 1.4×10^7 and 1.6×10^7 gold nanoparticles per hour, respectively, increasing by 1.7-fold to 2.3×10^7 nanoparticles per hour for MDA-MB-231 cells in agreement with the spectroscopy experiments. However, comparison of the total gold nanoparticles per cell indicates that both Du145 and MDA-MB-231 cells endocytose comparable quantities, resulting in 1.6×10^8 and 1.3×10^8 gold nanoparticles, respectively, over 24 hours. Despite exhibiting a similar rate of uptake during the 6-hour time period, L132 cells endocytosed significantly ($P = 0.03$) fewer gold nanoparticles,

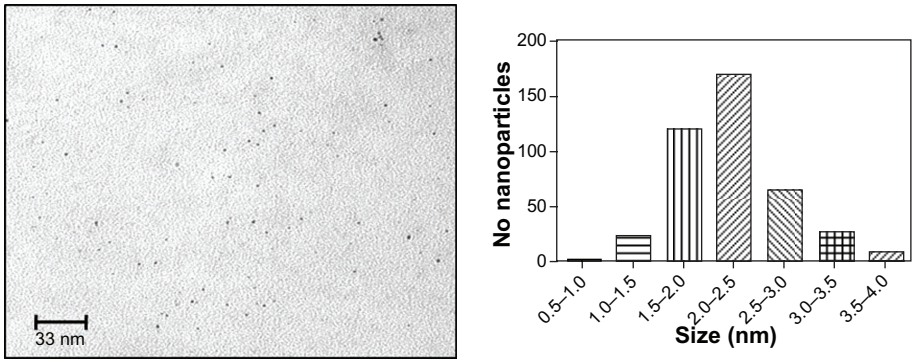

Figure 1 Transmission electron microscopic image of monodispersed 1.9 nm Aurovist™ gold nanoparticles.
Note: Normal distribution of gold nanoparticle size variation, with a median particle size ranging between 2.0 nm and 2.5 nm.

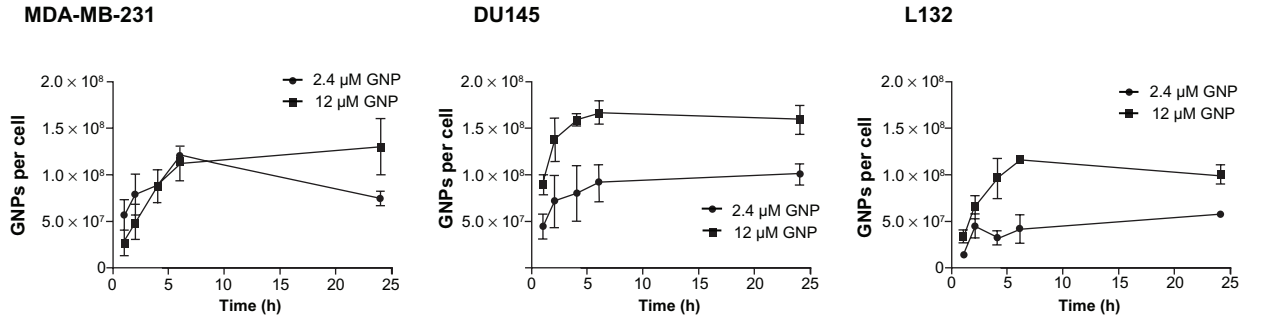

Figure 2 Determination of 1.9 nm gold nanoparticle uptake in MDA-MB-231 breast cancer cells, DU145 prostate cancer cells, and L132 immortalized normal cells.
Notes: Gold nanoparticles per cell calculated from atomic emission spectroscopy. Gold nanoparticle uptake was measured over a 24-hour period at either 2.4 μM or 12 μM. Results are shown as the mean ± standard error (n = 3).
Abbreviation: GNP, gold nanoparticles.

equating to 38% fewer total gold nanoparticles than DU145 cells. These differences are attributed to the higher rate of uptake in DU145 cells during the first hour of exposure to the nanoparticles. Furthermore, calculation of the intracellular gold concentration demonstrates an ability of the cell to hyperconcentrate gold. DU145 and MDA-MB-231 cells exposed to 12 μM (500 μg/mL of growth medium) accumulated intracellular gold concentrations of 8.4 mg/mL and 6.9 mg/mL, respectively, ie, approximately 17-fold and 14-fold greater than the exposure concentration.

Immunogold confocal microscopy

1.4 nm Alexa Fluor 488 FluoroNanogold™ was used to gain an insight into the gross distribution of gold nanoparticles within a cell. Figure 3A presents typical images of MDA-MB-231, DU145, and L132 cells following a 24-hour

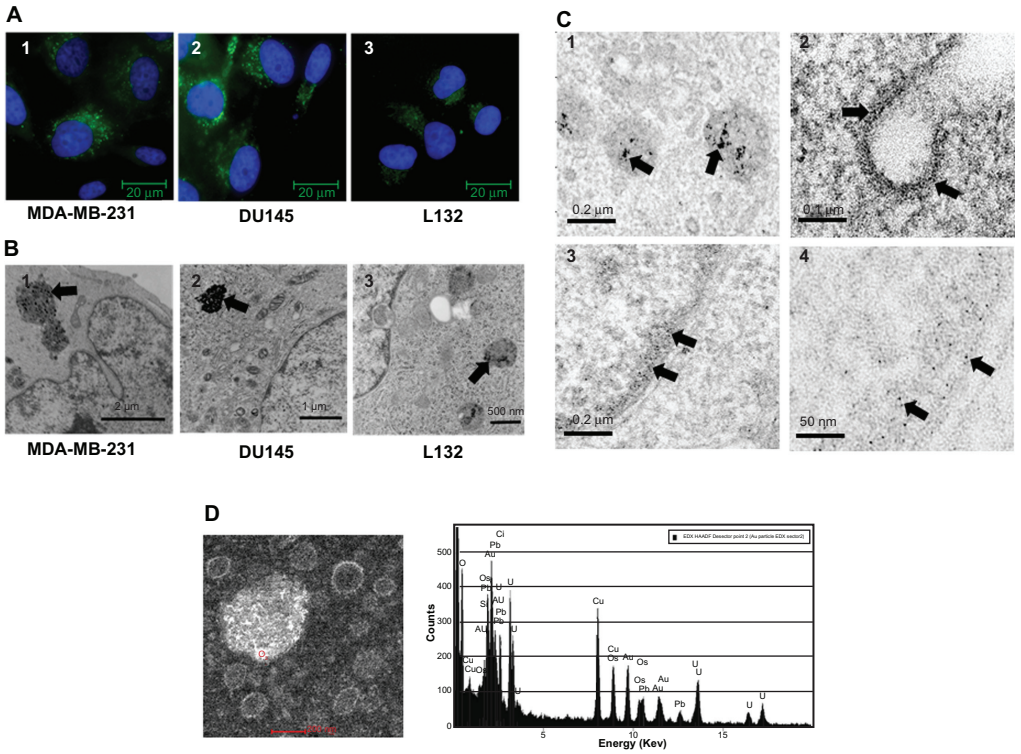

Figure 3 (**A**) Intracellular localization of 1.4 nm gold nanoparticles tagged with Alexa Fluor® 488. Gold nanoparticles were incubated for 24 hours at a 1:10 dilution of the stock solution resulting in perinuclear nuclear localization of the gold nanoparticles. Panels 1–3 represent MDA-MB-231, DU145, and L132 cells, respectively. (**B**) Intracellular localization of 1.9 nm particles localized to large endosomal bodies. Panels 1–3 represent MDA-MB-231, DU145, and L132 cells, respectively. (**C**) Field emission transmission electron microscopy images of MDA-MB-231 cells exposed to 12 μM of 1.9 nm gold nanoparticles. Panel 1 represents gold nanoparticles confined to endosomes within the cytoplasm. Panel 2 demonstrates an invaginated clathrin-coated pit with electron-dense material coating the cell membrane. Panels 3 and 4 represent intranuclear regions containing high-electron material. Arrows indicate gold nanoparticles and gold nanoparticle aggregates. (**D**) Confirmation of gold nanoparticle localization was obtained by scanning transmission electron microscopy and energy-dispersive x-ray spectroscopy.

exposure to medium containing 8 μg/mL FluoroNanogold. Qualitatively, the amount of fluorescence appeared to correlate with the ICP-AES measurements, with MDA-MB-231 and DU145 exhibiting higher fluorescence signals compared with L132 cells after a 24-hour exposure. Time course studies indicated cytoplasmic localization of the FluoroNanogold in the DU145 and MDA-MB-231 cells within one hour of exposure, with no fluorescent signal detectable in L132 cells before the 6-hour time point. In all cases, nanoparticle localization appeared to be constrained to cytoplasmic regions of the cell with areas of high intensity. This was particularly evident in the two tumor cell lines, with regions of greater intensity observed in the perinuclear protoplasm. However, despite these similarities, differences in the surface coating of FluoroNanogold and the presence of a fluorophore may significantly alter the intracellular distribution, necessitating comprehensive TEM study.

TEM and energy dispersive x-ray spectroscopy

TEM was used to determine the intracellular distribution of 1.9 nm gold nanoparticles following a 24-hour exposure at 12 μM. Figure 3B (panels 1–3) is representative of typical conventional TEM micrographs obtained using a Phillips CM 100 TEM at 100 kV. MDA-MB-231 and DU145 cells exhibited large secondary lysosomal structures packed with aggregates of a highly electron-dense material, which were confirmed to be gold aggregates using energy dispersive x-ray spectroscopy (Figure 3D). In keeping with the published literature, these gold nanoparticle lysosomes were constrained to the cytoplasm (Figure 3B). Evidence corroborating the observed difference in gold nanoparticle uptake by L132 cells was also observed by TEM. The characteristic large secondary lysosomal structures noted in the MDA-MB-231 and DU145 cells were much less densely packed, suggesting that L132 cells exhibit reduced endocytotic capacity. As with the MDA-MB-231 and DU145 tumor cells, no localization with other cytoplasmic organelles or the nuclear membrane was observed. High resolution images of MDA-MB-231 cells were obtained using the FEI Technai F20 TEM field emission transmission electron microscope (Figure 3C). To improve image quality and limit vesicle and endosome saturation, cells were exposed to 2.4 μM of 1.9 nm gold nanoparticles for a maximum of 6 hours. As with conventional TEM, secondary lysosomal bodies were observed 6 hours following exposure, and exhibiting typical aggregates (Figure 3C, panel 1). However, we also found evidence of nonendosomal intracellular gold nanoparticle distribution. Areas of comparatively diffuse, high electron-dense material were observed coating the outer membrane of an invaginated clathrin pit, with several intracytoplasmic vesicles appearing to demonstrate gold nanoparticles associated with their outer membrane (Figure 3C, panel 2). Interestingly, we also observed some of this material localized within the nucleus, exhibiting an apparent preference for heterochromatin accumulation. However, due to the relatively low nuclear concentrations compared with the dense endosome aggregations and the sensitivity limitations of energy dispersive x-ray spectroscopy analysis, we could not achieve a positive gold signal confirming the presence of gold nanoparticles distributed within the nucleus (Figure 3C, panel 4).

Cell growth assay

Cell growth curves were used to determine the effect of 12 μM 1.9 nm gold nanoparticles on cytokinesis (Figure 4A). Total cell numbers were fitted to an exponential growth equation, from which cell doubling time and the 95% confidence interval (CI) were calculated. A significant ($P = 0.0007$) retardation of cell growth was observed in the MDA-MB-231 cells 72 hours after gold nanoparticle exposure, with cell doubling time increasing from 22.7 hours (95% CI 21–25) for control cells to 29 hours (95% CI 23–38) for gold nanoparticle-treated cells. No significant difference in cell growth rates were observed in either the DU145 or L132 cell lines.

MTT cell proliferation assay

The MTT assay was used to assess the effect of gold nanoparticle concentration on cell viability in the same three cell lines as shown in Figure 4A. A dose-dependent reduction in cell viability was observed in DU145 and MDA-MB-231 cell lines, with LD_{50} values of 838 ± 11 μg/mL (20 μM) and 1028 ± 11 μg/mL (24.6 μM), respectively. L132 cells were much more resistant to 1.9 nm gold nanoparticles, with an extrapolated LD_{50} value of 13,300 ± 130 μg/mL (320 μM) (Figure 4B). The MTT assay was also used to corroborate cell growth curve findings following exposure to the 1.9 nm gold nanoparticles. All cell types were exposed to 12 μM gold nanoparticles for 24 hours and assayed at various time points up to 72 hours. MDA-MB-231 cells exhibited a significant ($P = 0.03$) reduction in viability compared with controls after as little as 24 hours after gold nanoparticle treatment, with cytostatic growth characteristics persisting out to 72 hours following treatment. Neither DU145 nor L132 cells exhibited any significant effect in relation to viability as determined by MTT assay.

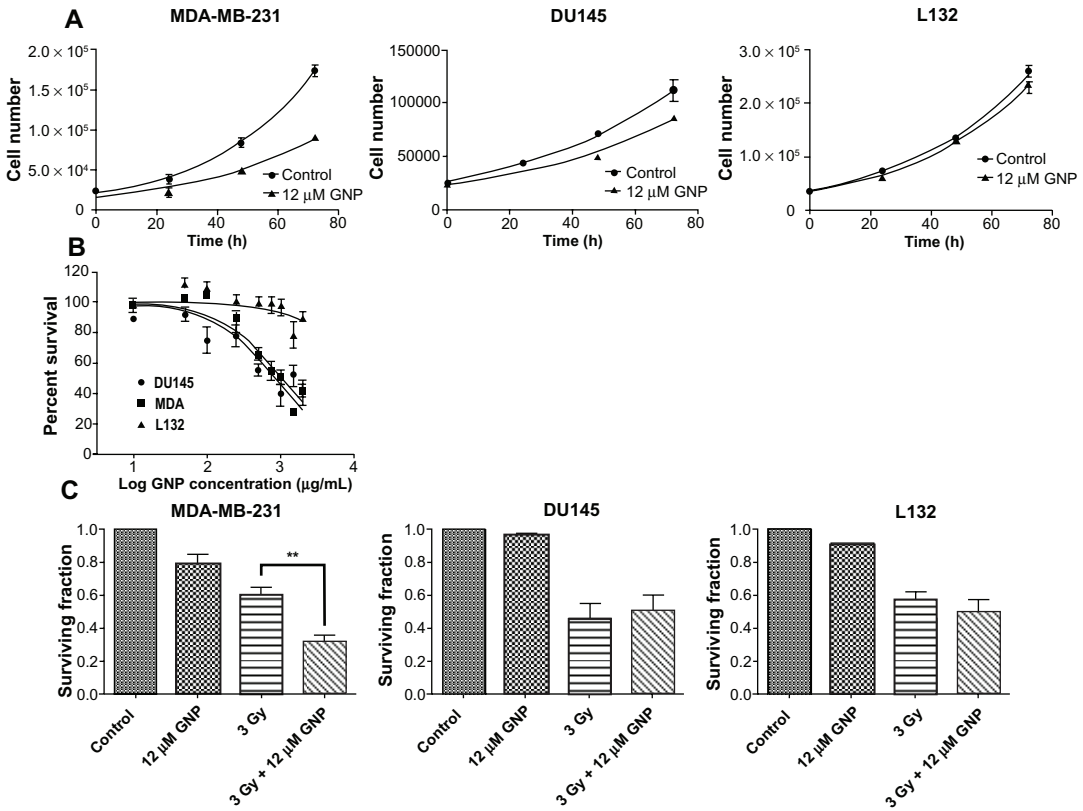

Figure 4 Determination of gold nanoparticle-induced cell growth inhibition and cytotoxicity. (**A**) Cell growth curves for MDA-MB-231, DU145, and L132 cells following a 24-hour exposure to medium containing 12 μM gold nanoparticles. (**B**) MTT assay of cell viability in DU145, MDA-MB-231, and L132 cells with increasing 1.9 nm gold nanoparticle concentrations. L132 cells are much more resistant to gold nanoparticles than the malignant cell lines, with LD_{50} values calculated at 838 ± 11 (20 μM), 1028 ± 11 (24.6 μM), and 13,300 ± 130 μg/mL (320 μM), respectively. (**C**) Cytotoxicity and radiosensitization potential determined by clonogenic assay following a 24-hour exposure to medium containing 12 μM gold nanoparticles. Irradiated cells were given a 3 Gy dose of 160 kVp x-rays. Colonies were fixed and stained after 2 weeks. Statistical significance was calculated using the two-tailed unpaired *t*-test, with a *P* value of ≤0.05 considered to be statistically significant.
Abbreviation: GNP, gold nanoparticles.

Clonogenic assay

Colony-forming assays were used to determine the long-term cytotoxic and radiosensitizing potential of 1.9 nm gold nanoparticles (Figure 4C). A significant ($P = 0.01$) cytotoxic effect was observed in MDA-MB-231 cells following a 24-hour exposure to 12 μM gold nanoparticles, equating to a 21% reduction in surviving fraction. No significant reduction in the colony-forming potential of DU145 or L132 cells was observed following exposure to gold nanoparticles. MDA-MB-231 cells treated with 12 μM GMP were significantly ($P = 0.002$) more sensitive to 3 Gy x-ray than control cells, increasing the therapeutic efficacy by 87%. No significant enhancement of radiation sensitivity was observed in the DU145 or L132 cells.

Expression of proapoptotic proteins

Western blot analysis was used to determine if exposure to gold nanoparticles induced expression of various proapoptotic-related proteins. Procaspase-9 (47 kDa), one of the late apoptosis-initiating proteins of the intrinsic pathway, was analyzed, along with the effector PARP, a DNA repair enzyme commonly cleaved as a result of caspase-3 and caspase-7 activation. In MDA-MB-231 cells (Figure 5A), a reduction in full length caspase-9 and PARP was observed from as early as 30 minutes after exposure to the gold nanoparticles, extending for the duration of the time course. Furthermore, there was a corresponding increase in the 89 kDa cleaved PARP fragment containing the catalytic and automodification domains. Likewise, in DU145 cells, but to a lesser extent, increases in both cleaved caspase-9 and cleaved PARP were evident after 24 hours, indicating that this concentration of gold nanoparticles was sufficient to induce an apoptotic response. After loading control correction, no increased cleavage of caspase-9 or PARP was observed in L132 cells.

Flow cytometry

Propidium iodide, a fluorescent DNA intercalating agent, was used to stain and quantify the proportion of cells in the

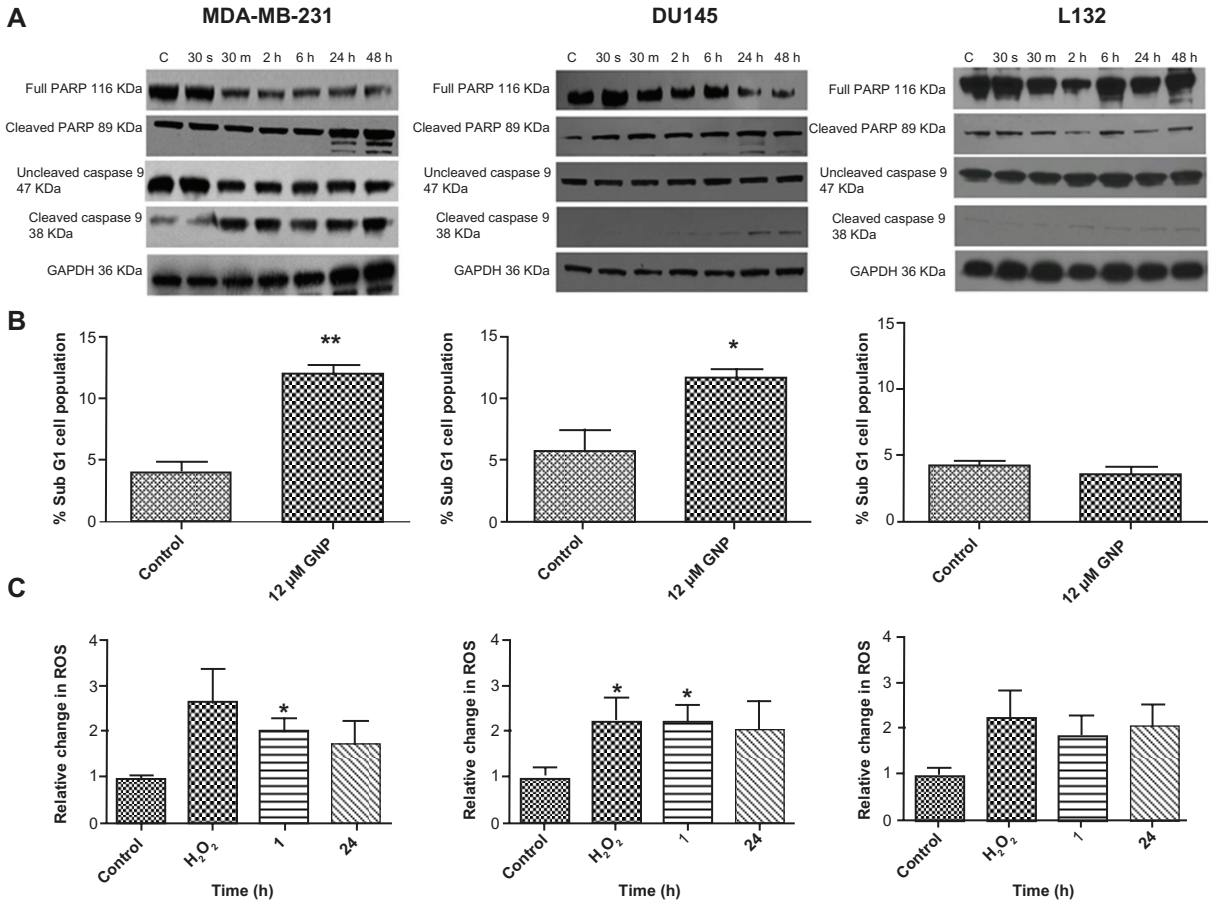

Figure 5 Mechanisms of 1.9 nm gold nanoparticle-induced cytotoxicity. (**A**) Western blot analysis determining levels of proapoptotic proteins, including PARP and caspase-9. (**B**) Flow cytometry analysis using propidium iodide to quantify the proportion of sub G_1 cells, indicating loss of cell viability. (**C**) Quantification of reactive oxygen species production following exposure to medium containing 12 μM gold nanoparticles for either 1 hour or 24 hours. Untreated controls and H2O2 samples were collected along with the 24 hour samples 24 hours. Statistical significance was calculated using the two-tailed unpaired *t*-test, with a *P* value of ≤0.05 considered to be statistically significant.
Abbreviation: GNP, gold nanoparticles.

sub G_1 phase of the cell cycle, indicative of nonviable cells. A significant ($P = 0.003$ and $P = 0.02$) increase by 2.9-fold and 2.0-fold in the sub G_1 cell population of MDA-MB-132 and DU145 cells, respectively, was observed, following a 24-hour treatment with 12 μM gold nanoparticles. This finding is in agreement with the increased expression of various proapoptotic proteins, and confirms that this preparation of gold nanoparticles induces cell death in these tumor cell line models. No increase, in the sub G_1 cell population was observed in the L132 cell line, providing further evidence that 1.9 nm gold nanoparticles do not induce any loss of viability in these immortalized normal cells.

Measurement of reactive oxygen species

We measured the relative change in generation of reactive oxygen species in the three cell lines following gold nanoparticle exposure to determine if the nanoparticles resulted in production of reactive oxygen species and if this was correlated with the observed cytotoxic and apoptotic findings. There was a significant ($P = 0.0132$ and $P = 0.0196$) increase in reactive oxygen species production in both the MDA-MB-231 and DU145 cells, respectively, one hour after treatment with 12 μM gold nanoparticles. Furthermore, levels of reactive oxygen species remained elevated over a 24-hour period. In keeping with the cytotoxic and apoptotic data, treatment with 12 μM gold nanoparticles failed to increase generation of reactive oxygen species significantly in L132 immortalized lung epithelial cells.

Discussion

Radiation absorption by high (Z) atomic number materials resulting in production of various secondary electron species is generally credited as being the mechanism of gold nanoparticle radiosensitization. Therefore, the amount of gold nanoparticles within a given cell and the distribution of these particles should directly impact upon the degree of radiosensitization. We have demonstrated that gold nanoparticle uptake occurs in a concentration-, time-, and

cell type-dependent manner. We report biphasic uptake characteristics, with maximal uptake occurring within the first few hours of exposure, reaching a plateau phase after 6 hours. This is consistent with the data reported by Chithrani et al,[19] who postulated that serum proteins bind to the surface of citrate-stabilized gold nanoparticles, producing a more stable gold nanoparticle-protein complex, capable of interacting with cell surface receptors.[19] Alterations in culture conditions (eg, temperature and intracellular adenosine triphosphate levels) significantly inhibited cellular uptake in that study, highlighting the energy-dependent nature of gold nanoparticle uptake. The precise uptake mechanism was elucidated using manipulation of intracellular sucrose and potassium levels, known to disrupt the clathrin-mediated endocytosis pathway.[20,30]

Nanoparticle size has also been shown to be closely associated with uptake potential, where clathrin-mediated endocytosis is the main entry route for particles up to 200 nm, after which caveolae-mediated endocytosis dominates.[31] Current data suggest that the optimal size for clathrin-mediated endocytosis falls between 25 nm and 50 nm, with a reduced uptake potential for extremely small (<10 nm) or extremely large (>100 nm) particles.[20,32,33] Using Herceptin® conjugated to gold nanoparticles (Her-gold nanoparticles), Jiang et al[34] demonstrated that 40 nm Her-gold nanoparticles exhibit a higher receptor binding affinity (about three orders of magnitude) for cell surface receptors than do 2 nm Her-gold nanoparticle complexes.[34]

Direct comparisons of our own data with previously published work is complicated due to the number of variables, including cell type, exposure time, concentration, and particle size. Table 1 details the individual experimental conditions of various studies and compares the total number of gold atoms per cell and the intracellular gold concentration with the current data. Despite the fact that a 1.9 nm gold nanoparticle contains just 213 atoms, calculations derived from our ICP-AES results indicate that MDA-MB-231 cells endocytose between 5000 and 10,000 times more gold nanoparticles per cell compared with previously published citrate stabilized particles.[19] Furthermore, calculations of the total number of gold atoms per cell indicate comparative uptake potentials, irrespective of size. Furthermore, the hyperconcentration of intracellular gold demonstrates active uptake of the particles to concentrations many times greater than initially exposed to. This has positive downstream implications in relation to the development of a clinically relevant particle by reducing the amount of gold nanoparticles required to achieve therapeutic gain. In our TEM studies, the presence of large endosomal aggregates, formed by the fusion of cytosolic vesicles with lysosomes, suggests that the majority of 1.9 nm particles are endocytosed in a relatively unaggregated state and subsequently fuse with endosomes to form the larger intracellular aggregates. Furthermore, consistent with the lower gold nanoparticle uptake potential of L132 cells, these endosomal aggregates were fewer and less densely packed than those observed in the tumor cell lines. This suggests that, in addition to the enhanced permeation and retention effect described in vivo by Maeda et al,[35] tumor cells also exhibit a higher endocytotic capacity, though further studies using other cell lines, both malignant and normal, will be required to determine this with confidence.[35,36]

The potential of gold nanoparticles as radiosensitizers through the generation of secondary electrons is directly affected by intracellular localization because the distance from the critical cellular target (DNA) will determine the efficacy of the secondary electrons. Nanodosimetry modeling carried out by our group indicates that approximately 90% of the secondary electron species generated from a

Table 1 Comparison of existing uptake data for various gold nanoparticle preparations, total nanoparticles per cell, and absolute number of total gold atoms per cell

Study	Cell type	GNP diameter (nm)	Atoms per AuNP	Maximum GNP per cell	Au atoms per cell	Intracellular Au conc (mg/ml)
Coulter et al (current study)	MDA-MB-231	1.9	213	1.31E + 08	2.79E + 10	6.9
Coulter et al (current study)	DU145	1.9	213	1.59E + 08	3.39E + 10	8.4
Coulter et al (current study)	L132	1.9	213	1.15E + 08	2.4E + 10	5.9
Chithrani et al[19]	HeLa	14	85390	3000	2.25E + 08	0.06
Chithrani et al[19]	HeLa	50	3890000	6160	2.40E + 10	5.94
Chithrani et al[19]	HeLa	74	12610000	2988	3.77E + 10	9.33
Nativo et al[39]	HeLa	16	127431	3.34E + 04	4.256E + 09	1.05

Note: Statistical significance calculated using the two-tailed unpaired *t*-test, with a *P* value of ≤0.05 considered significant.

10 nm gold nanoparticle are low-energy electrons (1.5 kV), increasing the dose deposition by 100-fold within a radius of less than 40 nm from the gold nanoparticle surface. The remaining high-energy electrons (>10 kV) account for approximately 10% of the secondary electrons produced, with a maximum range of >10 μm.[37] Endosomal entrapment of the gold nanoparticles within the cytosol prevents nuclear localization; however, various groups have attempted with some success to localize the gold nanoparticles within the nucleus, thereby increasing DNA damage and ultimately the formation of lethal double-strand breaks.[38–41] Using field emission TEM, we observed the characteristic localization of gold nanoparticles within the endosome as previously described (Figure 3C, panel 1). However, we also observed small (<5 nm) electron-dense particles in an unaggregated state inside the nuclear membrane (Figure 3C, panels 3 and 4). It should be noted that we failed to obtain a positive gold energy dispersive x-ray spectroscopy signature due to the sparse distribution of the material; however, studies of the nuclear pore complex indicate that small particles less than 9 nm are capable of both entering and exiting the eukaryotic nucleus via the nuclear pore complex by active diffusion.[42,43] Therefore, if the material presented in Figure 3C does represent intranuclear 1.9 nm gold nanoparticles, the use of small gold nanoparticles (<9 nm) would negate the need to add an additional level of complexity of specific nuclear targeting in the development of a candidate gold nanoparticle for systemic delivery.

Reports of gold nanoparticle cytotoxicity are conflicting, and have been attributed to a variety of factors, including surface coating, nanoparticle charge, and size.[21,23,24,44] Perhaps the strongest evidence for gold nanoparticle cytotoxicity is associated with particle size. Two similar gold nanoparticle preparations differing only in size showed very different cytotoxic profiles. Gold nanoparticles of size 1.4 nm capped with triphenylphosphine monosulfate were 100-fold more toxic than a 15 nm nanoparticle comprising identical components.[45] Conversely, Hondroulis et al[46] assessed the cytotoxicity of a 10 nm and a 100 nm gold nanoparticle using an electrical impedance whole cell assay. In this instance, the authors failed to observe any difference in the growth potential between gold nanoparticle-treated cells and control cells.[46] Our findings corroborate much of the existing literature, in that an oversimplified conclusion, such as gold nanoparticles are either nontoxic or cytotoxic, fails to account for a variety of subtle yet important factors. We consistently demonstrated significant impaired growth characteristics, a reduction in cell viability, and a loss of clonogenicity in MDA-MB-231 cells following exposure to 12 μM 1.9 nm gold nanoparticles for a 24-hour period. However, immortalized normal L132 cells failed to exhibit any notable cytotoxicity. Although likely to be a contributing factor, different uptake potentials should not be solely attributed to cytotoxicity, because the total gold concentration per DU145 cell is greater than that of an MDA-MB-231 cell, and although uptake was lower, L132 cells consistently internalize approximately 60% of the maximum number of gold nanoparticles endocytosed by a DU145 cell. Interestingly, the correlation between maximum uptake and potential radiosensitization did not directly relate to the differential uptake potential, with MBA-MB-231 cells being the only cell line model investigated exhibiting significant gold nanoparticle-induced radiosensitization.

We examined expression levels of various proteins associated with apoptosis to establish if 1.9 nm gold nanoparticles promoted cell death via this pathway. An increase in both cleaved caspase-9 and cleaved PARP was observed in MDA-MB-231 and DU145 cells, correlating with a reduction in cell growth and clonogenicity. Furthermore, no detectable upregulation of these proteins was detected in L132 cells. Analysis of the sub G_1 cell population further corroborated the Western blot findings, indicating that apoptosis was the likely mode of cell death. As with other aspects of gold nanoparticle research, variables in experimental design often result in contrasting conclusions. A recent study by Kang et al[41] demonstrated significant cytotoxicity of 30 nm gold nanoparticles conjugated with a nuclear localization signal, resulting in increased γ-H2aX phosphorylation (a surrogate marker of DNA double-strand breaks) and an accumulation of cells in the sub G_1 phase of the cell cycle. The authors concluded that gold nanoparticle nuclear localization resulted in arrest of cytokinesis, with an increased apoptotic cell population following exposure to gold nanoparticles.[41] However, in another study, pretreatment of cells with Z-VAD-*fmk*, a caspase inhibitor, failed to rescue cells following exposure to a high concentration (96 μM, $2 \times LD_{50}$) of a 1.4 nm gold nanoparticle preparation, suggesting that necrosis, and not apoptosis, was the predominant pathway at this concentration. Addition of the antioxidants, N-acetylcysteine and glutathione, abrogated the effect, leading the authors to conclude that gold nanoparticles at high concentrations cause oxidative stress via increased production of endogenous reactive oxygen species and depletion of intracellular antioxidants.[45] We directly measured reactive oxygen species production using 2DCFDA, and observed an increase in MDA-MB-231 and DU145 cells which correlated with increased cytotoxicity and all of the apoptotic endpoints investigated. Despite the lack of

a significant increase in generation of reactive oxygen species in L132 cells, the consistent trend towards elevated reactive oxygen species indicates a role for the induction of gold nanoparticle-induced oxidative stress, with our tumor cell models indicating a higher degree of sensitivity to oxidative damage. This biological phenomenon adds further credence to the findings by Jain et al[17] who described radiosensitization using gold nanoparticles at MV energies and suggested that, in addition to the physical process of radiosensitization, due to the differences in the absorption coefficient between gold and soft tissue, there may be additional biological effects responsible for radiosensitization.[17]

In conclusion, there is clear variability between the uptake potential of the cell lines investigated. While it is interesting that the immortalized normal cell line did not endocytose gold nanoparticles as efficiently as the tumor cell lines, studies in a much broader range of cells will be needed to determine if there is a consistent difference. Strong evidence for biological sensitization is provided by the localization of gold nanoparticles within the cytoplasm, thereby limiting the DNA-damaging capabilities of low energy secondary electrons. This is further substantiated by our previous findings that gold nanoparticles induced no significant increase in double-strand break formation, and bleomycin, a radiomimetic agent, in the presence of 12 μM gold nanoparticles, resulted in a sensitizer enhancement ratio of 1.38.[17] Although significant cytotoxicity was observed in MDA-MB-231 cells, resulting in a 21% reduction in clonogenicity, cytotoxicity in the remaining cell lines was less than 10%. We believe that the cytotoxicity observed does not limit the usefulness of this gold nanoparticle preparation as a potential sensitizing modality, because current radiosensitizing agents, such as cisplatin and cetuximab, exhibit much greater levels of normal cell damage.[47,48]

Acknowledgments

The authors thank Pat Larkin in the School of Medicine and Dentistry and Stephen McFarland in the School of Mathematics and Physics for technical assistance with the TEM. They also thank Cancer Research UK for financial support of this work (grants C1278/A990 to DGH and C1513/A7047 to KMP).

Disclosure

The authors report no conflicts of interest in this work.

References

1. Lee CM, Jang D, Cheong SJ, et al. Surface engineering of quantum dots for in vivo imaging. *Nanotechnology*. 2010;21(28):285102.
2. Fan D, Yin Z, Cheong R, et al. Subcellular-resolution delivery of a cytokine through precisely manipulated nanowires. *Nat Nanotechnol*. 2010;5(7):545–551.
3. Chen J, Saeki F, Wiley BJ, et al. Gold nanocages: bioconjugation and their potential use as optical imaging contrast agents. *Nano Lett*. 2005;5(3):473–477.
4. Hirsch LR, Stafford RJ, Bankson JA, et al. Nanoshell-mediated near-infrared thermal therapy of tumors under magnetic resonance guidance. *Proc Natl Acad Sci U S A*. 2003;100(23):13549–13554.
5. Loo C, Lin A, Hirsch L, et al. Nanoshell-enabled photonics-based imaging and therapy of cancer. *Technol Cancer Res Treat*. 2004;3(1):33–40.
6. Hainfeld JF, Slatkin DN, Smilowitz HM. The use of gold nanoparticles to enhance radiotherapy in mice. *Phys Med Biol*. 2004;49(18):N309–N315.
7. Hainfeld JF, Slatkin DN, Focella TM, Smilowitz HM. Gold nanoparticles: a new x-ray contrast agent. *Br J Radiol*. 2006;79(939):248–253.
8. Shi X, Wang S, Meshinchi S, et al. Dendrimer-entrapped gold nanoparticles as a platform for cancer-cell targeting and imaging. *Small*. 2007;3(7):1245–1252.
9. Brown SD, Nativo P, Smith JA, et al. Gold nanoparticles for the improved anticancer drug delivery of the active component of oxaliplatin. *J Am Chem Soc*. 2010;132(13):4678–4684.
10. Terentyuk GS, Maslyakova GN, Suleymanova LV, et al. Laser-induced tissue hyperthermia mediated by gold nanoparticles: toward cancer phototherapy. *J Biomed Opt*. 2009;14(2):021016.
11. Peng C, Zheng L, Chen Q, et al. PEGylated dendrimer-entrapped gold nanoparticles for in vivo blood pool and tumor imaging by computed tomography. *Biomaterials*. 2012;33(4):1107–1119.
12. Cho SH, Jones BL, Krishnan S. The dosimetric feasibility of gold nanoparticle-aided radiation therapy (GNRT) via brachytherapy using low-energy gamma-/x-ray sources. *Phys Med Biol*. 2009;54(16):4889–4905.
13. Zheng Y, Hunting DJ, Ayotte P, Sanche L. Radiosensitization of DNA by gold nanoparticles irradiated with high-energy electrons. *Radiat Res*. 2008;169(1):19–27.
14. McMahon SJ, Mendenhall MH, Jain S, Currell F. Radiotherapy in the presence of contrast agents: a general figure of merit and its application to gold nanoparticles. *Phys Med Biol*. 2008;53(20):5635–5651.
15. Regulla DF, Hieber LB, Seidenbusch M. Physical and biological interface dose effects in tissue due to X-ray-induced release of secondary radiation from metallic gold surfaces. *Radiat Res*. 1998;150(1):92–100.
16. Chithrani DB, Jelveh S, Jalali F, et al. Gold nanoparticles as radiation sensitizers in cancer therapy. *Radiat Res*. 2010;173(6):719–728.
17. Jain S, Coulter JA, Hounsell AR, et al. Cell-specific radiosensitization by gold nanoparticles at megavoltage radiation energies. *Int J Radiat Oncol Biol Phys*. 2011;79(2):531–539.
18. Leung MKK, Chow JCL, Chithrani BD, Lee MJG, Oms B, Jaffray DA. Irradiation of gold nanoparticles by x-rays: Monte Carlo simulation of dose enhancements and the spatial properties of the secondary electrons production. *Med Phys*. 2011;38(2):624–631.
19. Chithrani BD, Ghazani AA, Chan WC. Determining the size and shape dependence of gold nanoparticle uptake into mammalian cells. *Nano Lett*. 2006;6(4):662–668.
20. Chithrani BD, Chan WC. Elucidating the mechanism of cellular uptake and removal of protein-coated gold nanoparticles of different sizes and shapes. *Nano Lett*. 2007;7(6):1542–1550.
21. Connor EE, Mwamuka J, Gole A, Murphy CJ, Wyatt MD. Gold nanoparticles are taken up by human cells but do not cause acute cytotoxicity. *Small*. 2005;1(3):325–327.
22. Shukla R, Bansal V, Chaudhary M, Basu A, Bhonde RR, Sastry M. Biocompatibility of gold nanoparticles and their endocytotic fate inside the cellular compartment: a microscopic overview. *Langmuir*. 2005;21(23):10644–10654.
23. Goodman CM, McCusker CD, Yilmaz T, Rotello VM. Toxicity of gold nanoparticles functionalized with cationic and anionic side chains. *Bioconjug Chem*. 2004;15(4):897–900.

24. Pan Y, Neuss S, Leifert A, et al. Size-dependent cytotoxicity of gold nanoparticles. *Small*. 2007;3(11):1941–1949.
25. Zhang XD, Guo ML, Wu HY, et al. Irradiation stability and cytotoxicity of gold nanoparticles for radiotherapy. *Int J Nanomedicine*. 2009;4:165–173.
26. Butterworth KT, Coulter JA, Jain S, et al. Evaluation of cytotoxicity and radiation enhancement using 1.9 nm gold particles: potential application for cancer therapy. *Nanotechnology*. 2010;21(29):295101.
27. Hainfeld JF, Dilmanian FA, Zhong Z, Slatkin DN, Kalef-Ezra JA, Smilowitz HM. Gold nanoparticles enhance the radiation therapy of a murine squamous cell carcinoma. *Phys Med Biol*. 2010;55(11): 3045–3059.
28. Gu YJ, Cheng J, Lin CC, Lam YW, Cheng SH, Wong WT. Nuclear penetration of surface functionalized gold nanoparticles. *Toxicol Appl Pharmacol*. 2009;237(2):196–204.
29. Puck TT, Marcus PI. Action of x-rays on mammalian cells. *J Exp Med*. 1956;103(5):653–666.
30. Kam NW, Liu Z, Dai H. Carbon nanotubes as intracellular transporters for proteins and DNA: an investigation of the uptake mechanism and pathway. *Angew Chem Int Ed Engl*. 2006;45(4):577–581.
31. Rejman J, Oberle V, Zuhorn IS, Hoekstra D. Size-dependent internalization of particles via the pathways of clathrin- and caveolae-mediated endocytosis. *Biochem J*. 2004;377(Pt 1):159–169.
32. Gao H, Shi W, Freund LB. Mechanics of receptor-mediated endocytosis. *Proc Natl Acad Sci U S A*. 2005;102(27):9469–9474.
33. Zhang S, Li J, Lykotrafitis G, Bao G, Suresh S. Size-dependent endocytosis of nanoparticles. *Adv Mater*. 2009;21:419–424.
34. Jiang W, Kim BY, Rutka JT, Chan WC. Nanoparticle-mediated cellular response is size-dependent. *Nat Nanotechnol*. 2008;3(3):145–150.
35. Maeda H, Wu J, Sawa T, Matsumura Y, Hori K. Tumor vascular permeability and the EPR effect in macromolecular therapeutics: a review. *J Control Release*. 2000;65(1–2):271–284.
36. Choi MR, Stanton-Maxey KJ, Stanley JK, et al. A cellular Trojan Horse for delivery of therapeutic nanoparticles into tumors. *Nano Lett*. 2007;7(12):3759–3765.
37. McMahon SJ, Hyland WB, Muir MF, et al. Biological consequences of nanoscale energy deposition near irradiated heavy atom nanoparticles. *Sci Rep*. 2011;1:18.
38. Tkachenko AG, Xie H, Coleman D, et al. Multifunctional gold nanoparticle-peptide complexes for nuclear targeting. *J Am Chem Soc*. 2003;125(16):4700–4701.
39. Nativo P, Prior IA, Brust M. Uptake and intracellular fate of surface-modified gold nanoparticles. *ACS Nano*. 2008;2(8):1639–1644.
40. Xie W, Wang L, Zhang Y, et al. Nuclear targeted nanoprobe for single living cell detection by surface-enhanced Raman scattering. *Bioconjug Chem*. 2009;20(4):768–773.
41. Kang B, Mackey MA, El-Sayed MA. Nuclear targeting of gold nanoparticles in cancer cells induces DNA damage, causing cytokinesis arrest and apoptosis. *J Am Chem Soc*. 2010;132(5): 1517–1519.
42. Feldherr CM, Akin D. Regulation of nuclear transport in proliferating and quiescent cells. *Exp Cell Res*. 1993;205(1):179–186.
43. Allen TD, Cronshaw JM, Bagley S, Kiseleva E, Goldberg MW. The nuclear pore complex: mediator of translocation between nucleus and cytoplasm. *J Cell Sci*. 2000;113(Pt 10):1651–1659.
44. Sonavane G, Tomoda K, Makino K. Biodistribution of colloidal gold nanoparticles after intravenous administration: effect of particle size. *Colloids Surf B Biointerfaces*. 2008;66(2):274–280.
45. Pan Y, Leifert A, Ruau D, et al. Gold nanoparticles of diameter 1.4 nm trigger necrosis by oxidative stress and mitochondrial damage. *Small*. 2009;5(18):2067–2076.
46. Hondroulis E, Liu C, Li CZ. Whole cell based electrical impedance sensing approach for a rapid nanotoxicity assay. *Nanotechnology*. 2010;21(31):315103.
47. Brezden CB, Horn L, McClelland RA, Rauth AM. Oxidative stress and 1-methyl-2-nitroimidazole cytotoxicity. *Biochem Pharmacol*. 1998;56(3):335–344.
48. Bonner JA, Harari PM, Giralt J, et al. Radiotherapy plus cetuximab for squamous-cell carcinoma of the head and neck. *N Engl J Med*. 2006;354(6):567–578.